Evaluation of structure-borne and airborne noise in hydrogen-powered train engines

Braj Bhushan Prasad[1], Dmitrij Wintergoller[1], Tommy Luft[1], Hermann Rottengruber [1]

[1] *Institute for Engineering of Products and Systems, Otto-von-Guericke-University Magdeburg, 39106 Magdeburg, Germany*

[1] *Email: braj.prasad@ovgu.de, dmitrij.wintergoller@ovgu.de, tommy.luft@ovgu.de, hermann.rottengruber@ovgu.de*

Introduction

This paper examines the acoustic characteristics of hydrogen-powered internal combustion engines (ICEs) for railway applications. Hydrogen-powered trains offer a sustainable alternative to diesel engines, but noise emissions remain a challenge. Furthermore, to comply with EU noise regulations and ensure market acceptance, precise acoustic measurements are essential. A three-phase measurement approach is used: the first phase establishes a baseline without the powerpack, the second phase evaluates the powerpack's impact on noise, and the third phase analyzes noise under real operating conditions. This paper presents results from the first phase, laying the groundwork for further assessments and supporting the development of hydrogen-powered ICEs for railways. The research engine used for the measurements is shown in Figure 1. The test bench has dimensions of 19.3 m×7.4 m×8.3 m, with the vibrofoundation base area measuring 12.0 m × 2.9 m. The setup includes a water brake capable of handling engine power up to 3600 kW, along with towing equipment featuring a 500 kW electric machine. Additionally, the engine periphery is designed to support engine power up to 3000 kW, while the hydrogen periphery can supply engine power up to 1000 kW.

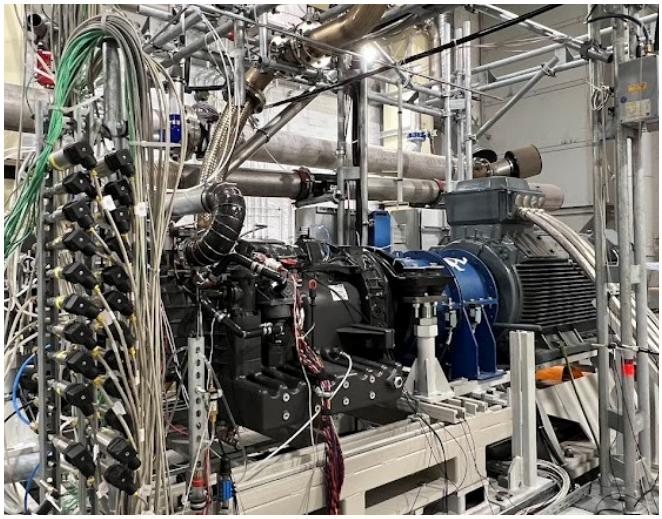

Figure 1: Internal combustion engine converted from a diesel variant to operate on hydrogen.

Conversion from diesel to Hydrogen operation

The hydrogen-powered engine utilized in this study was converted from its original diesel configuration. This section provides a concise overview of the key steps involved in the conversion process.

One of the main challenges with hydrogen combustion engines is their susceptibility to combustion anomalies, with knocking combustion being the most well-known. This is due to the extremely low minimum ignition energy of 0.017 mJ [1], which also promotes the risk of backfires or preignition.

To prevent backfires in the intake system, hydrogen can be directly injected into the combustion chamber. Therefore, the injection system was adapted from diesel to an H_2-DI A-injector. However, achieving ignition, known as "glow ignition", where the fuel-air mixture ignites at hot spots in the combustion chamber, remains a challenge. To counteract this, the compression ratio was reduced from 18 to 11.8 to prevent knocking. A delayed ignition timing can also decrease the tendency for knocking, but it results in a reduction in efficiency. Additionally, due to the higher self-ignition temperature of hydrogen, the ignition system was adapted by installing a spark plug.

Hydrogen has a high laminar flame speed of approximately 230 cm/ [1]. This property leads to rapid combustion and, consequently, a short burning duration, resulting in energy conversion occurring within a brief period. As a result, the combustion process approaches the ideal constant-volume process, leading to high process efficiency. The short burning duration also favors the stability of the combustion process, particularly with lean fuel-air mixtures [1]. However, a high flame speed leads to increased pressures and temperatures in the combustion chamber, which have disadvantages in terms of noise emissions, nitrogen oxide formation, and wall heat losses [1]. The consequences of higher pressures and temperatures in the combustion chamber, due to the shortened combustion time, result in higher torque and power output of the engine.

Hydrogen as a fuel has a significant advantage, especially in today's environmental awareness: The combustion of H2 theoretically produces no carbon compounds such as CO2, CO, or HC. The only significant pollutant emissions during hydrogen combustion are nitrogen oxides, which are particularly pronounced under slight excess air, high combustion temperatures, and longer residence times in the post-flame zone of the combustion chamber.

To ensure low-emission hydrogen combustion, a fuel-air ratio of $\lambda > 2$ should be preferred [1]. The wide flammability limit of hydrogen with $0.13 < \lambda < 10$ [1], which allows for controlled operation throughout the engine map, also enables lean operation. It should be noted that in lean operation, there is an excess of air in the combustion chamber that is not involved in the combustion pro-

cess and can reduce the combustion chamber temperature through heat absorption. The engine was measured on the research engine at the WTZ Roßlau GmbH test bench. The engine test bench is shown in Figure 1. The technical specifications of the research engine are detailed in Table 1.

Table 1: Geometric data of the research engine.

Parameters	Values
Number of cylinders	6
Displacement	12.8 dm^3
Stroke	166 mm
Bore	128 mm
Compression ratio	11.8:1
Nominal peak power	390 kW

Figure 2 illustrates the in-cylinder pressure variation as a function of crank angle, highlighting the combustion process and its associated acoustic effects. The pressure curve exhibits a rapid increase, peaking near the top dead center (TDC), followed by a gradual decline as the combustion gases expand. The ignition timing threshold (ITT) is marked before TDC, indicating the initiation of combustion.

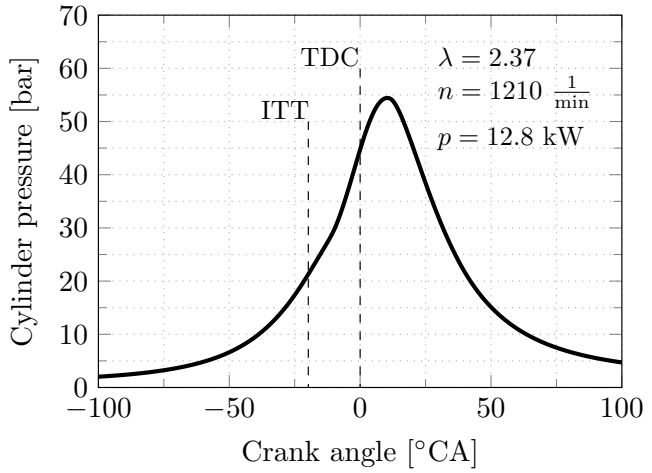

Figure 2: Cylinder pressure oscillations during combustion vs. crank angle at 72 kW and 1210 RPM.

The evolution of in-cylinder pressure during combustion exhibits rapid fluctuations that directly impact its frequency spectrum, as shown in Figures 3 and 4. The spectral peaks correspond to specific frequency components of the pressure oscillations depicted in Figure 2. The maximum pressure is associated with lower-frequency sound emissions, the pressure rise corresponds to mid-frequency sound emissions, and the rate of pressure rise is linked to higher-frequency sound emissions.

Experimental studies

To assess the structure-borne noise characteristics of the hydrogen-powered engine, measurements were conducted at three distinct bearing points of the engine. In order to capture the structure-borne sound, a three-dimensional (3D) accelerometer was securely mounted at each of these

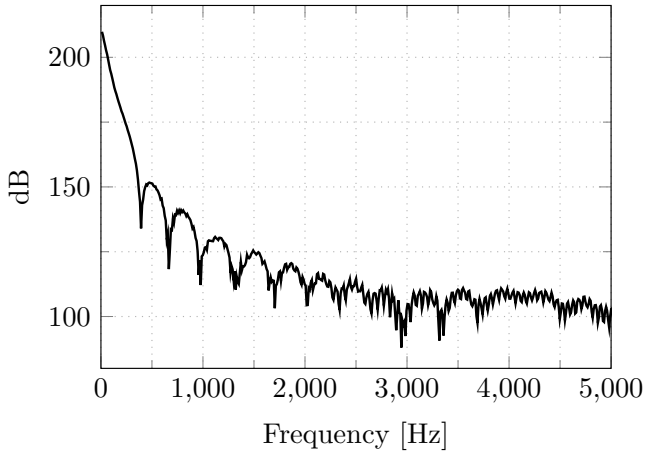

Figure 3: Cylinder pressure excitation spectrum in the frequency domain, presented on a dB scale.

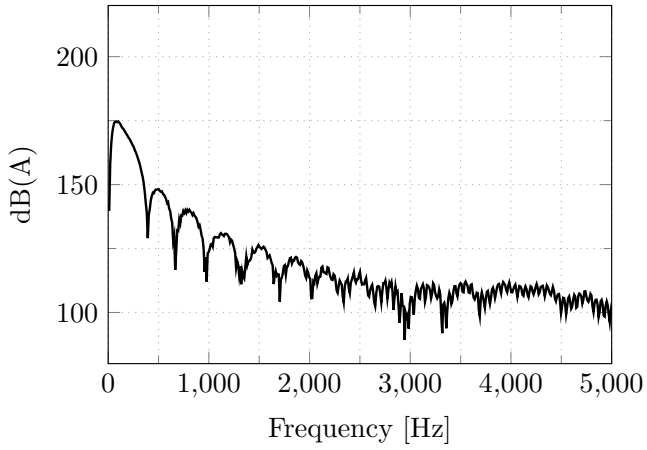

Figure 4: Cylinder pressure excitation spectrum in the frequency domain, presented on a dB(A) scale.

bearing points. The placement of the accelerometers was chosen to ensure accurate and representative data collection regarding the vibrational behavior of the engine at these critical locations. A detailed illustration of the sensor positioning is provided in Figure 5.

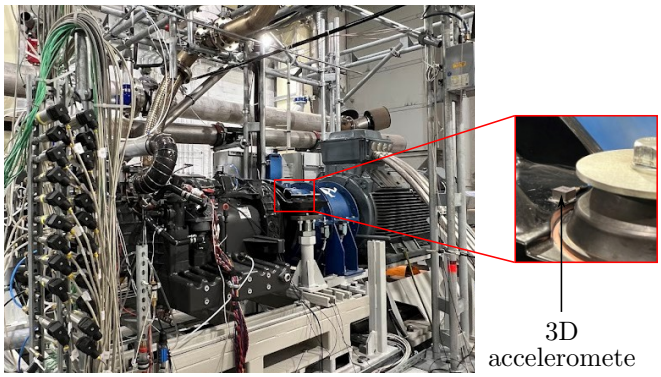

Figure 5: Experimental setup for measuring structure-borne sound.

Figure 6 shows the experimental setup for measuring

airborne sound from the engine, using a 12-microphone array positioned around the test object to capture the sound pressure distribution in 3D space. This configuration allows for determining the machine's radiated sound power. The 12 measurement positions follow ISO 6798-1:2020-02 standards, ensuring consistency and accuracy. A detailed schematic of the microphone arrangement is provided in Figure 7. Each microphone is mounted on a tripod for stability and alignment, minimizing errors from movement or vibrations. A self-leveling 360° cross-line laser is used to accurately position the microphones, projecting reference lines to ensure precise measurement grid setup and adherence to required distances and angles.

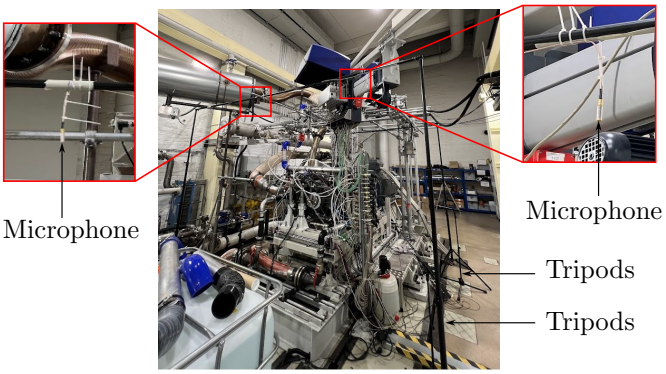

Figure 6: Experimental setup for measuring airborne sound.

The dimensions of the rectangular measuring surface, as illustrated in Figure 7, were carefully measured to ensure accuracy in the subsequent calculations. The measured lengths include l_1, l_2, and l_3, alongside the specific dimensions denoted as a, b, c, d, e, and f. These values serve as fundamental parameters for determining the total surface area of the measurement setup. The measured values are presented in Table 2.

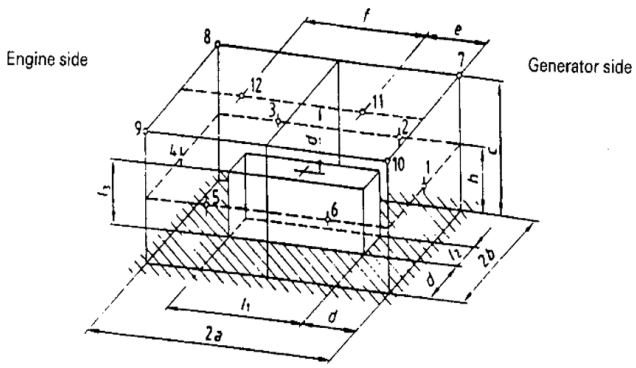

Figure 7: Configuration of twelve measurement points and the measurement surface.

Table 2: Dimensions of the rectangular measuring surface.

Parameters	a	b	c	d	e	f	h	l_1	l_2	l_3
Value [m]	1.42	1.33	2.46	1.00	0.71	1.42	1.23	1.54	0.66	1.46

Using these measured values, the total surface area (S) is computed using the following equation:

$$S = 2 \cdot 2a \cdot c + 2 \cdot 2b \cdot c + 2a \cdot 2b = 34.61 \text{ m}^3 \quad (1)$$

It is important to note that the experiment is conducted outside an anechoic chamber. However, the influence of environmental factors on the recorded measurements is mitigated through the application of a correction factor, as discussed in the results section.

Results

This study focuses on a hydrogen-based engine adapted from a diesel counterpart. It evaluates both structure-borne and airborne noise characteristics of the modified engine, comparing them to the original diesel version. Sound power, an intrinsic property unaffected by external factors, is used as the primary acoustic parameter for objective and reliable comparison. This ensures standardized assessments and allows a comprehensive evaluation of the hydrogen engine's acoustic performance.

The sound power can be calculated using the following equation:

$$L_w = L_p + L_S + K_0 + K_1 - K_2, \quad (2)$$

where, L_p represents the sound pressure level on the measuring surface, L_S denotes the dimensions of the measuring surface, K_0 is the characteristic impedance correction, and K_1 and K_2 correspond to the external noise and environmental corrections, respectively. The measuring surface dimensions L_S is given by:

$$L_S = 10 \cdot lg \frac{S}{S_0}, \quad (3)$$

where S denotes the measuring surface area and S_0 represents the reference surface area, with S_0 being assigned a value of 1 m^2. The characteristic impedance K_0 can be computed by using the following expression:

$$K_0 = -10 \cdot lg \frac{Z}{Z_0} = -10 \cdot lg \frac{\rho \cdot c}{(\rho \cdot c)_0}. \quad (4)$$

In Equation (4), Z denotes the acoustic impedance of the medium, and Z_0 represents the reference impedance. The impedance value can be calculated using the medium's density and the velocity of sound within it. Z_0 has been determined based on the physical framework and is set to a fixed value of 400 $\frac{\text{Ns}}{\text{m}^3}$. The parameter Z was calculated as a function of ambient temperature to account for its dependency on environmental conditions. Using this temperature-dependent formulation, K_0 was subsequently computed to ensure accuracy in the analysis.

As mentioned earlier, the experiments were conducted outside an anechoic chamber. Therefore, external noise and environmental corrections are necessary. These corrections can be calculated using Equations (5) and (6), respectively. In these equations, ΔL represents the difference between the measured and background noise, and A denotes the equivalent absorption area, which can be computed using the room volume (V) and reverberation time (T).

Table 3: Sound power of hydrogen and diesel ICE under varying operating conditions.

Operating point	RPM	Load [Nm]	L_w lin dB (Hydrogen ICE)	L_w dB(A) (Hydrogen ICE)	L_w dB(A) (Diesel ICE)
1	600	140	107.97	99.90	99.50
2	600	300	108.80	100.88	102.70
3	600	500	111.00	101.56	-
4	650	130	107.90	99.49	100.50
5	650	260	108.18	99.41	102.40
6	650	500	110.40	101.38	-
7	700	120	107.73	99.53	101.70
8	700	240	108.48	99.87	103.50
9	700	510	111.46	101.91	-
10	750	100	107.81	99.33	100.30
11	750	240	108.82	99.88	104.90
12	750	510	111.34	102.43	-
13	800	107	108.26	100.08	101.10
14	800	297	109.16	100.72	106.40
15	800	500	112.43	102.74	-
16	1210	570	112.71	104.84	105.70

$$K_1 = -10 \cdot lg\left(1 - 10^{(-0.1\,\Delta L)}\right). \tag{5}$$

$$K_2 = 10 \cdot lg\left(1 + 4 \cdot \frac{S}{A}\right), \tag{6}$$

with

$$A = 0.163 \cdot \frac{V}{T}. \tag{7}$$

The computed sound power for 16 different operating conditions is presented in Table 3. It is evident that, in general, the hydrogen-powered ICE generates lower noise levels compared to its diesel counterpart. However, for operating point 1, the difference in sound power between the hydrogen and diesel ICE is minimal. Thus, it can be concluded that the hydrogen ICE is slightly quieter than the diesel version. It is important to note, however, that the hydrogen ICE does not have a powerpack attached, whereas the diesel ICE is equipped with one, which contributes to its sound emission. Therefore, in the next phase of the project, measuring the hydrogen ICE with a powerpack will be essential to facilitate a direct comparison between the two engine types.

Figure 8 illustrates a clear decrease in structure-borne sound velocity levels from 130 dB at 63 Hz to 90 dB at 10 kHz. High levels and step-like drops below 315 Hz suggest strong low-frequency transmission with potential resonances. A gradual reduction occurs from 315 Hz to 1 kHz, followed by stabilization at 90 dB above 3.15 kHz, indicating effective high-frequency attenuation.

Summary and outlook

This paper explores the acoustic properties of hydrogen-powered ICEs for railway transport. The results demonstrate that the hydrogen-powered ICE generally produces lower noise levels than its diesel counterpart, with sound power measurements showing the hydrogen engine to be slightly quieter under most operating conditions. However, the comparison is not entirely equitable, as the hydrogen ICE was tested without a powerpack, while the diesel ICE was equipped with one, which influences its sound emissions. To ensure a direct and fair comparison, the next phase of the project will involve testing the hydrogen ICE with a powerpack. This study aims to contribute to the development of hydrogen-powered ICEs for railway applications by offering a comprehensive understanding of their acoustic behavior.

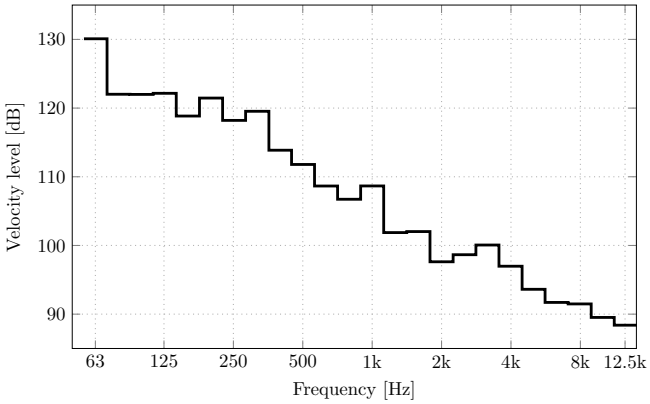

Figure 8: Averaged velocity levels in the z-direction for structure-borne sound from three sensors at 72 kW, 1210 RPM.

Acknowledgement

The authors thank the Federal Ministry of Education and Research for supporting this work within the joint project "TRAINS UV15 - Trainset demonstrator with H2 combustion and health monitoring". Special thanks to Torsten Winkler for his invaluable assistance with the measurements.

References

[1] Wintergoller, D.; Dafis, A.; Rottengruber, H.: Analysis of Hydrogen Combustion in a Commercial Vehicle Engine Using 1D Simulation and Subsequent CFD Simulation, SAE technical paper (2023).

[2] Rottengruber, H.: Untersuchung der Stickoxidbildung an einem Wasserstoff-Dieselmotor, Technische Universität München (1999).